Unconventional magnification behaviour in microsphere-assisted microscopy

Stephane Perrin[1], Hongyu Li, Sylvain Lecler, Paul Montgomery

ICube laboratory, University of Strasbourg - CNRS, 67412 Illkirch, France

Abstract

Microsphere-assisted microscopy is an original sub-diffraction-limit imaging technique allowing to reach a few hundred nanometres of lateral resolution in air by only placing a microbead in a classical optical microscope. This work aims to highlight the magnification process in microsphere-assisted microscopy which behaves differently than in optical microscopy. As a matter of fact, the lateral magnification of an optical microscope does not change according to focus plane positions. Experiments on the super-resolution imaging technique, performed in air through soda-lime-glass microspheres and attested by simulations, demonstrate a significant increase in the magnification factor along the microsphere imaging depth, *i.e.* at different object-focal-plane position of the objective. Moreover, it is shown that the magnification range, as well as its slope, depend on the size of the microsphere. In addition, the influence of the spectral width of the illumination light source on the magnification range is highlighted.

Keywords: Microscopy; Super-resolution; Microsphere; Magnification; Image formation

1. Introduction

Resolving power in classical optical microscopy is limited by diffraction of light, resulting in a minimal distance between two distinct object details of half of the wavelength in air using a low-coherent illumination [1]. The idea of sub-diffraction-limit imaging techniques appeared with the need to visualize increasingly smaller elements [2], and with the notion of *ultra-microscopy* [3]. Several super-resolution imaging techniques have then been developed in the last century such as confocal microscopy [4, 5] (further enhanced using a double-pass configuration [6] and the photonic jet phenomenon [7]), scanning near-field optical microscopy [8, 9], structured illumination microscopy [10, 11] and metamaterials-based superlenses [12, 13]. They contributed to bringing optical nanoscopy to the forefront reinforced by the Nobel Prize for Chemistry in 2014 with super-resolved fluorescence microscopy [14] and single molecule localization microscopy [15]. Nevertheless, these super-resolution imaging techniques require high stability systems, complex alignment or long acquisition time.

In 2011, Z. Wang *et al.* experimentally demonstrated full-field label-free super-resolution microscopy **using low-refractive-index microspheres (silica microspheres with n $\sim$ 1.46)** [16]. Relatively easy-to-implement, this approach consists in introducing a transparent microsphere in a classical white-light microscope, *i.e.* between the sample and the microscope objective. A magnified image, providing sub-diffraction-limit information, is then generated and collected by the microscope. **In the past years, several papers have focused on performance of the super-resolution imaging technique. In 2012, A. Darafsheh *et al.* suggested placing high-refractive-index microspheres (barium-titanate-glass with n $\sim$ 2.0) in an immersion liquid [17] and, more recently, embedding in an elastomer layer [18]. The studies of the immersion medium influence on the image contrast [19, 20] and on the image nature [21, 22], as well as of the role of the coherence of light on the lateral resolution [23, 24], lead to a better understanding of the imaging technique. In addition, the manipulation of the microspheres has been studied, making it possible to perform**

[1]Corresponding author: Stephane Perrin,
Email address: stephane.perrin@unistra.fr

contact-less super-resolution measurements [25, 26, 27, 28]; methods which could, for example, avoid to damage biological samples during the acquisitions [29, 30, 31]. These contributions are promising in fabrication of novel optical devices (*e.g.*, microsphere-embedded microscope accessories), enabling to improve optical microscopy.

Experimentally, microsphere-assisted microscopy is able to reach a lateral resolution higher than confocal microscopy and solid immersion lens [32], and similar to structured illumination microscopy and negative-index superlenses [33]. However, being a recent imaging technique, some phenomena are still not fully explained such as the origin of the super-resolution resolving power. Due to the micron-scale size of the spheres, their imaging properties do not exactly follow geometrical optics [34, 35] and theoretical analyses remain thus complex. A possible collection of the evanescent waves by the microsphere followed by their conversion in the far field appears relevant yet to explain the super-resolving power [36, 37]. In microsphere-based nanoscopy, not only the super-resolution phenomenon is still not fully explained, but also the image process. Unlike optical microscopy, microsphere-assisted microscopy provides long axial focusing ranges, therefore the imaging factor within the imaging depth behaves in an unconventional way. As a matter of fact, the lateral magnification differs according to the axial position of the microscope objective. As an example, Supplementary Movie illustrates the change in the magnification along the optical axis using a soda-lime-glass microsphere with a diameter of 29 µm. This effect could lead to divergent interpretations of results (*e.g.*, the magnification from a 4.7-µm-diameter microsphere equals ×4.1 and even ×8 in Ref [16], and ×2.8, in Ref [28]). Therefore, a range of magnification factor is sometimes preferred in order to avoid any position-dependent-magnification confusions [29, 38].

This work exposes a fundamental property in microsphere-assisted microscopy by highlighting the non-classical evolution of the lateral magnification along the imaging depth. Through experimental measurements and numerical analyses, the influence of the microsphere diameter, as well as the bandwidth of the light source, on the magnification behaviour is shown in air.

2. Methods

A classical optical microscope in reflecting mode has thus been enhanced by introducing glass microspheres (Cospheric LLC, California) having different diameters. **The soda-lime-glass microspheres have a refractive index of 1.52.** The illumination part consists of a white-light source (λ_0 = 650 nm, $\Delta\lambda$ = 400 nm) where the emitting beam passes through a Köhler arrangement to provide a more homogeneous intensity distribution. The field diaphragm has been closed to improve the imaging contrast [39]. In addition, wavelength filters (a cyan filter with λ_0 = 567 nm and $\Delta\lambda$ = 90 nm, and a blue-line filter with λ_0 = 445 nm and $\Delta\lambda$ = 11 nm) can be introduced in order to limit the spectral width of the light source. The object beam is then directed towards the imaging part and passes through the transparent microsphere and the microscope objective (Zeiss, ×50, NA = 0.55), as shown in Fig. 1(a). Here, the object is a contrast grating target having a period of 400 nm (fabricated at the MIMENTO Technology Centre, FEMTO-ST Institute, France). It can be noted that the optical microscope alone is not able to visualize the 200-nm-groove-width features (Fig. 1(b)). Indeed, considering the transfer function of the whole white-light microscope, the resolving power equals only 840 nm. The microsphere is thus placed in air on the surface of the object, allowing the super-resolution phenomenon to occur. A camera finally records the super-resolution image

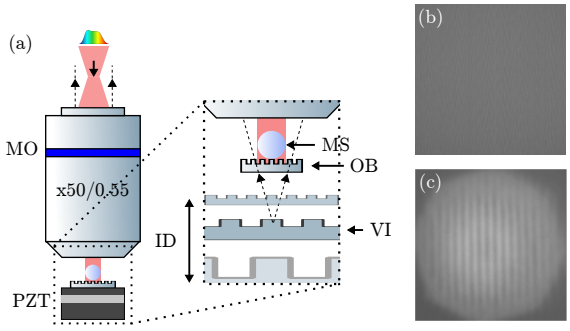

Figure 1: (a) Layout of optical head of the microsphere-based nanoscope. A microscope objective (MO) collects the virtual image (VI) of the object (OB) which was magnified before by a 25-µm-diameter glass microsphere (MS). A piezoelectric device (PZT) allows the MO to focus on different axial VI planes along the imaging depth (ID) by displacing OB and MS. Comparison of performance between (b) the MO alone and (c) the MS-based nanoscope, by imaging a 200-nm-linewidth grating.

(Fig. 1(c)) from the objective lens and a relay lens. In order to capture the virtual images at different positions along the optical axis, a piezoelectric device is vertically displaced. The depth of field of the microscope objective (∼ 1 µm) defines the axial sampling of the measurements. **During the experiments, the measurements were repeated using ten similar microspheres. For example, experimental curve represented in Fig. 2(a) results thus of an averaging of the magnification factors through ten 25-µm-diameter microspheres. Moreover, at each axial position, the magnification measurements were performed ten times.**

3. Results and Discussion

The lateral magnification generated by the microsphere, defined as the ratio between the grating periods in the image plane and the object plane, was first measured according to the axial position where the objective focuses on (Fig. 2(a)). A soda-lime-glass microsphere having a diameter of 25 µm was used to demonstrate the influence of the axial image position on the magnification factor. A linear evolution along the microsphere imaging depth (∼ 60 µm) is shown, changing from ×4 to ×8 while maintaining the super-resolution phenomenon. This effect is significantly different to conventional full-field optical system. Indeed, the magnification of a conventional optical microscope remains constant over the clearest imaging depth. Obviously, the virtual images at positions deeper than 60 µm have a contrast decreased (Fig. 2(b.iii)). In order to confirm the experimental results, a rigorous 2D electromagnetic model was also implemented by using a finite element method (Comsol Multiphysics). The simulation of super-resolution virtual imaging consists in two steps [23, 40, 41]: firstly, the electric fields from the object, *i.e.* two point sources, interacts with a microsphere. Then, the transmitted electric field is time-reverse propagated in free-space, *i.e.* propagated in the opposite axial direction without the microsphere, in order to retrieve the two images. The broadband illumination of the light source is considered by repeating the two steps over the visible spectral range ($\Delta\lambda$ = 400 nm, step = 50 nm) and then the wavelength-dependant irradiance distributions are summed (Fig. 2(c)). The simulated magnification factor, *i.e.* the transverse distance ratio between the two resulting

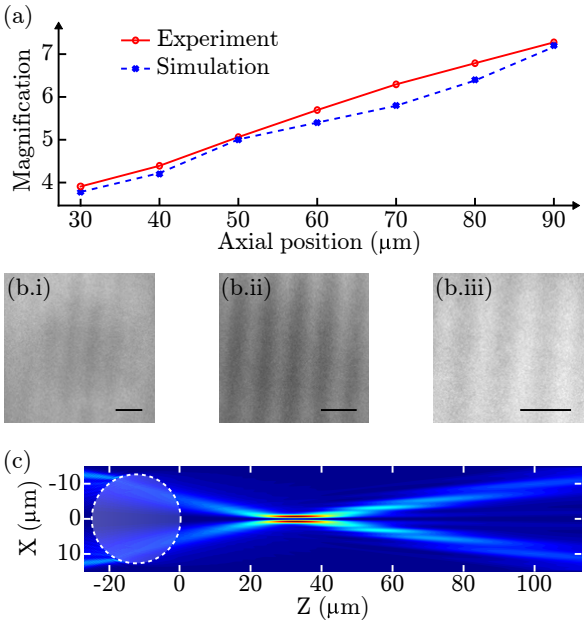

Figure 2: (a) Experimental (red solid line) and numerical (blue dotted line) evolutions of the lateral magnification from a 25-µm-diameter microsphere placed in air using a white-light source, along the microbead imaging depth (Z axial position). (b.i), (b.ii) and (b.iii) are the virtual images of the 400 nm periodic object at Z positions of 30 µm, 55 µm and 90 µm, respectively. Scale bars represent 1 µm. (c) Simulation of the virtual image formation. The object is two point sources placed against the microsphere. The white dotted line illustrates the initial microsphere location.

images and the two point sources, is represented by the blue dotted line in Fig. 2(a) according to the longitudinal position of the image plane, showing magnification values in good agreement with the experiments.

Afterwards, the influence of the microsphere diameter on the position-dependent magnification were studied. Eight glass microspheres having different diameters were hence placed on the 400-nm-period grating. **In order to be readable, Fig. 3(a) represents the linear evolution of the magnification factor for only three microsphere diameters, *i.e.* 7 µm, 46 µm and 125 µm.** The curves allow to affirm that, at a given axial image position, the large microspheres provide a magnification factor lower than when using small microspheres. Moreover, the microsphere-diameter dependence on the magnification curve slope α has been estimated and is represented in Fig. 3(b) (red-color curve). A fitting curve is juxtaposed, highlighting the inverse proportionality of the slope α

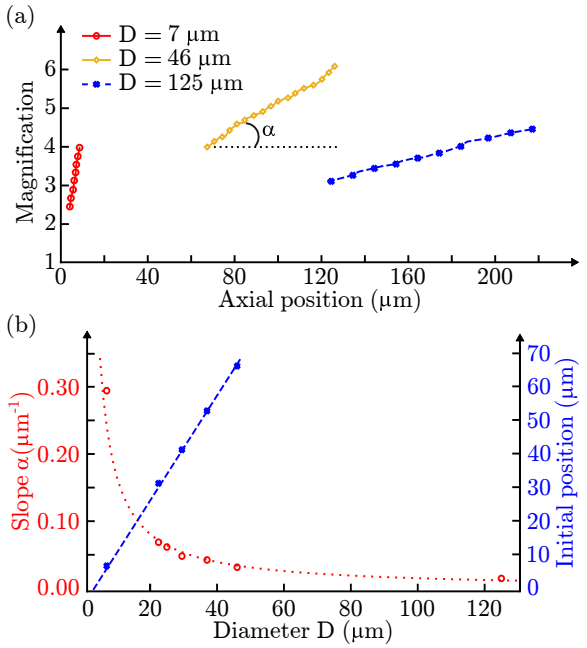

Figure 3: (a) Evolution of the lateral magnification in air from microspheres having diameters of 7 µm (in red), 46 µm (in orange) and 125 µm (in blue), as a function of axial position Z. The microspheres are illuminated by a white-light source. (b) Evolution of the magnification inclination α (in red) and the initial image position (in blue) for different diameters D. A curve fitting $1/D$ function is superimposed to the calculated values α.

according to the diameter D of the soda-lime-glass microspheres. In air and using soda-lime-glass microspheres, this relation is expressed as:

$$\alpha[\text{in } \mu\text{m}^{-1}] = \frac{1.83}{D[\text{in } \mu\text{m}]} \qquad (1)$$

In addition, Fig. 3(a) shows that the smaller the diameter, the narrower the imaging depth is. Indeed, not only the magnification factor but also the imaging depth are highly affected by the size of the microsphere. The large microspheres are able to form virtual images at deeper positions, requiring to focus with the microscope objective at further positions. The linear proportionality of the initial position of the imaging depth as a function of the diameter of soda-lime-glass microspheres is shown in Fig. 3(b) (blue-color curve).

Finally, the role of the spectral bandwidth of the light source on the magnification was investigated. For this purpose, the performance of the 25-µm-diameter microsphere using the white light source (represented by the red line in Fig 4) is compared with two spectrally-gated illuminations, *i.e.* using the cyan filter (cyan line) and the blue-line-filter (blue line). The magnification factor remains linearly proportional according to the axial position and magnification values do not differ regardless of the spectral bandwidth of the light source. However, only the magnification range appears limited. As a matter of fact, the smaller the spectral bandwidth is, the narrower the microsphere imaging depth. This assumption can be retrieved through glass microspheres having another diameter.

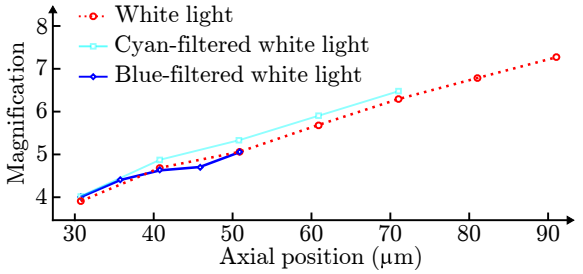

Figure 4: Evolution of the lateral magnification from a 25-µm-diameter microsphere placed in air as a function of axial position under three types of light source having 400 nm (in red line), 90 nm (in cyan line) and 11 nm (in blue line) of bandwidth.

In this work, the unconventional behaviour of the lateral magnification in microsphere-assisted microscopy has been achieved in air using soda-lime-glass microspheres. It should however be mentioned that this effect occurs also using microspheres having a higher refractive index and in a different immersion configuration [35, 42].

4. Conclusions

This work exposes a fundamental property in microsphere-assisted microscopy: the non-classical behaviour of the lateral image magnification. Contrary to classical optical microscopy, the magnification factor is subject to a linear evolution along the microsphere imaging depth, and both geometrical and optical parameters have an influence on the position-dependent magnification slope and range. Indeed, through experiments and numerical simulations, it has been shown that the microsphere size is inversely proportional to the magnification growth and is linearly proportional to the initial position of the axial field of view. Furthermore, the reduction of the spectral bandwidth of the illumination light source indeed limits the magnification range.

Acknowledgements

The authors thank A. Leong-Hoi for her fruitful contribution. This work received funding from SATT Conectus Alsace and was partly supported by the French RENATECH network (FEMTO-ST Institute, Besançon) and the University of Strasbourg.

References

[1] H. von Helmholtz and H.E. Fripp, On the limits of the optical capacity of the microscope, Monthly Microscopical Journal **16** (1876) 15-39. doi:10.1111/j.1365-2818.1876.tb05606.x.

[2] Editorial, Beyond the diffraction limit. Nature Photon. **3** (2009) 361. doi:10.1038/nphoton.2009.100.

[3] E.H. Synge, A suggested method for extending microscopic resolution into the ultra-microscopic region, Phil. Mag. 7 **6** (1928) 356-362. doi:10.1080/14786440808564615.

[4] H. Goldmann, Spaltlampenphotographie und photometric, Ophthalmologica **98** (1939) 257-270. doi:10.1159/000299716.

[5] H. Naora, Microspectrophotometry and cytochemical analysis of nucleic acids, Science **114** (1951) 279. doi:10.1126/science.114.2959.279.

[6] C.J.R. Sheppard and Y. Gong, Improvement in axial resolution by interference confocal microscopy, Optik **87** (1991) 129-132.

[7] Z. Chen, A. Taflove, and V.Backman, Photonic nanojet enhancement of backscattering of light by nanoparticles: a potential novel visible-light ultramicroscopy technique, Opt. Express **12** (2004) 1214-1220. doi:10.1364/OPEX.12.001214.

[8] E.A. Ash and G. Nicholls, Super-resolution aperture scanning microscope, Nature **237** (1972) 510-512. doi:10.1038/237510a0

[9] D. Courjon, *Near-field microscopy and near-field optics* (Imperial College Press, London, 2003).

[10] W. Lukosz and M. Marchand, Optischen Abbildung Unter Uberschreitung der Beugungsbedingten Auflsungsgrenze, Opt. Acta. **10** (1963) 241-255. doi:10.1080/713817795.

[11] M. Saxena, G. Eluru, and S.S. Gorthi, Structured illumination microscopy, Adv. Opt. Photon. **7** (2015) 241-275. doi:10.1364/AOP.7.000241.

[12] V.G. Veselago, The electrodynamics of substances with simultaneously negative values of ϵ and μ, Sov. Phys. Usp. **10** (1968) 509-514. doi:10.1070/PU1968v010n04ABEH003699.

[13] X. Zhang and Z. Liu, Superlenses to overcome the diffraction limit, Nat. Mater. **7** (2008) 435-441. doi:10.1038/nmat2141.

[14] S.W. Hell, Far-field optical nanoscopy, Science **316** (2007) 1153-1158. doi:10.1126/science.1137395.

[15] R.M. Dickson, A.B. Cubitt, R.Y. Tsien, and W.E. Moerner, On/off blinking and switching behaviour of single molecules of green fluorescent protein, Nature **388** (1997) 355-358. doi:10.1038/41048.

[16] Z. Wang, W. Guo, L. Li, B. Luk'yanchuk, A. Khan, Z. Liu, Z. Chen, and M. Hong, Optical virtual imaging at 50 nm lateral resolution with a white-light nanoscope, Nat. Commun. **2** (2011) 218. doi:10.1038/ncomms1211.

[17] A. Darafsheh, G.F. Walsh, L. Dal Negro, and V.N. Astratov, Optical super-resolution by high-index liquid-immersed microspheres, Appl. Phys. Lett. **101** (2012) 141128 doi:10.1063/1.4757600.

[18] A. Darafsheh, C. Guardiola, A. Palovcak, J.C. Finlay, and A. Carabe, Optical super-resolution imaging by high-index microspheres embedded in elastomers, Opt. Lett. **40** (2015) 5-8. doi:10.1364/OL.40.000005.

[19] A. Darafsheh, Influence of the background medium on imaging performance of microsphere-assisted super-resolution microscopy, Opt. Lett. **42** (2017) 735-738 doi:10.1364/OL.42.000735.

[20] Y. Zhou, Y. Tang, Y. He, X. Liu, and S. Hu, Effects of immersion depth on super-resolution properties of index-different microsphere-assisted nanoimaging, Appl. Phys. Express **11** (2018) 032501. doi:10.7567/APEX.11.032501.

[21] L. Yao, Y.-H. Ye, H. Feng Ma, L. Cao, and J. Hou, Role of the immersion medium in the microscale spherical lens imaging, Opt. Commun. **335** (2015) 23-27. doi:10.1016/j.optcom.2014.08.051.

[22] H.S.S. Lai, F. Wang, Y. Li, B. Jia, L. Liu, and W.J. Li, Super-resolution real imaging in microsphere-assisted microscopy, PLoS ONE **11** (2016) e0165194. doi:10.1371/journal.pone.0165194.

[23] A.V. Maslov and V.N. Astratov, Imaging of sub-wavelength structures radiating coherently near microspheres, App. Phys. Lett. **108** (2016) 051104. doi:10.1063/1.4941030.

[24] S. Perrin, S. Lecler, A. Leong-Hoi, and P.C. Montgomery, Role of coherence in microsphere-assisted nanoscopy, Proc. SPIE **10330** (2017) 103300V. doi:10.1117/12.2270246.

[25] L.A. Krivitsky, J.J. Wang, Z. Wang, and B. Luk'yanchuk, Locomotion of microspheres for super-resolution imaging, Sci. Rep. **3** (2013) 3501. doi:10.1038/srep03501.

[26] J. Li, W. Liu, T. Li, I. Rozen, J. Zhao, B. Bahari, B. Kante, and J. Wang, Swimming microrobot optical nanoscopy, Nano Lett. **16** (2016) 6604-6609. doi:10.1021/acs.nanolett.6b03303.

[27] F. Wang, L. Liu, H. Yu, Y. Wen, P. Yu, Z. Liu, Y. Wang, and W.J. Li, Scanning superlens microscopy for non-invasive large field-of-view visible light nanoscale imaging, Nat. Commun. **7** (2016) 13748. doi:10.1038/ncomms13748

[28] M. Duocastella, F. Tantussi, A. Haddadpour, R.P. Zaccaria, A. Jacassi, G. Veronis, A. Diaspro, and F. De Angelis, Combination of scanning probe technology with photonic nanojets, Sci. Rep. **7** (2017) 3474. doi:10.1038/s41598-017-03726-5.

[29] L. Li, W. Guo, Y. Yan, S. Lee, and T. Wang, Label-free super-resolution imaging of adenoviruses by submerged microsphere optical nanoscopy, Light Sci. Appl. **2** (2013) e104. doi:10.1038/lsa.2013.60

[30] H. Yang, N. Moullan, J. Auwerx, and M.A.M. Gijs, Super-resolution biological microscopy using virtual imaging by a microsphere nanoscope, Small **10** (2014) 1712-1718. doi:10.1002/smll.201302942

[31] S. Perrin, H. Li, K. Badu, T. Comparon, G. Quaranta, N. Messaddeq, N. Lemercier, P. Montgomery, J.-L. Vonesch, and S. Lecler, Transmission microsphere-assisted dark-field microscopy. Phys. Status Solidi RRL.

(2018) 1800445. doi:10.1002/pssr.201800445.

[32] A. Darafsheh, N.I. Limberopoulos, J.S. Derov, D.E. Walker Jr., and V.N. Astratov, Advantages of microsphere-assisted super-resolution imaging technique over solid immersion lens and confocal microscopies, Appl. Phys. Lett. **104** (2014) 061117. doi:10.1063/1.4864760.

[33] X. Hao, C. Kuang, X. Liu, H. Zhang, and Y. Li, Microsphere based microscope with optical super-resolution capability, Appl. Phys. Lett. **99** (2011) 203102. doi:10.1063/1.3662010.

[34] A. Darafsheh, Optical super-resolution and periodical focusing effects by dielectric microspheres, Ph.D. dissertation, University of North Carolina at Charlotte (2013).

[35] S. Lecler, S. Perrin, A. Leong-Hoi, and P. Montgomery, Photonic jet lens, Submitted to Sci. Rep. (2018).

[36] Y. Duan, G. Barbastathis, and B. Zhang, Classical imaging theory of a microlens with super-resolution, Opt. Lett. **38** (2013) 2988-2990. doi:10.1364/OL.38.002988

[37] Y. Ben-Aryeh, Increase of resolution by use of microspheres related to complex Snell's law, J. Opt. Soc. Am. A **33** (2013) 2284-2288. doi:10.1364/JOSAA.33.002284

[38] S. Yang, F. Wang, Y.-H. Ye, Y. Xia, Y. Deng, J. Wang, and Y. Cao, Influence of the photonic nanojet of microspheres on microsphere imaging, Opt. Express **25** (2017) 27551-27558. doi:10.1364/OE.25.027551.

[39] S. Perrin, H. Li, A. Leong-Hoi, S. Lecler, and P. Montgomery, Illumination conditions in microsphere-assisted microscopy, Submitted to J. Microsc. (2018).

[40] S. Perrin, A. Leong-Hoï, S. Lecler, P. Pfeiffer, I. Kassamakov, A. Nolvi, E. Haeggström, and P. Montgomery, Microsphere-assisted phase-shifting profilometry, Appl. Opt. **56** (2017) 7249-7255. doi:10.1364/AO.56.007249.

[41] I. Kassamakov, S. Lecler, A. Nolvi, A. Leong-Hoi, P. Montgomery, and E. Haeggstrom, 3D Super-Resolution Optical Profiling Using Microsphere Enhanced Mirau Interferometry, Sci. Rep. **7** (2017) 3683. doi:10.1038/s41598-017-03830-6.

[42] H.C. Van de Hulst, *Light Scattering by Small Particles* (John Wiley & Sons, New York, 1957).